

## RESEARCH ARTICLE

10.1002/2013JD020149

## Key Points:

- Most climate models simulate diurnal peak in convective rainfall too early
- Problem can be fixed by allowing convection to start from more levels
- Simple modification of convective parameterization

## Correspondence to:

I. Folkins,  
ian.folkins@dal.ca

## Citation:

Folkins, I., T. Mitovski, and J. R. Pierce (2014), A simple way to improve the diurnal cycle in convective rainfall over land in climate models, *J. Geophys. Res. Atmos.*, 119, doi:10.1002/2013JD020149.

Received 8 MAY 2013

Accepted 3 FEB 2014

Accepted article online 5 FEB 2014

## A simple way to improve the diurnal cycle in convective rainfall over land in climate models

Ian Folkins<sup>1</sup>, T. Mitovski<sup>1</sup>, and J. R. Pierce<sup>1,2</sup>

<sup>1</sup>Department of Physics and Atmospheric Science, Dalhousie University, Halifax, Nova Scotia, Canada, <sup>2</sup>Department of Atmospheric Science, Colorado State University, Fort Collins, Colorado, USA

**Abstract** Within the tropics, and during the summer months in midlatitudes, most of the rainfall reaching the surface is generated by moist convection. Over land, the diurnal cycle in moist convective rainfall usually peaks in the late afternoon. In most climate models, the diurnal peak in convective rainfall occurs several hours too early and is often near local solar noon. We argue that this bias partly originates from the methods used in convective parameterizations to calculate the cloud base mass flux. In most convective parameterizations, the initial convective mass flux is determined from the convective available potential energy (CAPE) of an updraft parcel originating from the model layer closest to the surface. In models, the rapid increase in the CAPE of this near-surface layer following sunrise contributes to a rapid increase in convective precipitation. However, the mass-weighted CAPE of the boundary layer as a whole responds much more slowly to the increase in downward solar radiation at the surface. Using a recently developed convective parameterization in version 4 of the Community Atmosphere Model (CAM4), we show that the overall accuracy in the diurnal simulation of convective precipitation increases as the number of near-surface layers from which convective air parcels are permitted to originate increases from one to four. We also show that the simulation of the diurnal cycle in convective precipitation over land can be improved through the introduction of variables which attempt to represent the persistence of subgrid-scale convective organization within a grid column across model time steps.

### 1. Introduction

Most of the rainfall in the tropics, and in midlatitudes during the summer months, originates from convective clouds. Over land, convective rainfall exhibits a strong diurnal cycle, with a characteristic peak in the late afternoon or early evening [Nesbitt and Zipser, 2003]. This diurnal cycle gives rise to diurnal cycles in cloud amount [May *et al.*, 2012] and relative humidity [Soden, 2000] which modify the propagation of solar and thermal radiation through the troposphere and affect the surface radiation balance. Regional-scale sea breeze circulations, especially in the tropics, are usually strongly coupled to the diurnal variation in convective rainfall [Ploshay and Lau, 2010]. The boundary layer mixing ratios of many species, including carbon dioxide [de Arellano *et al.*, 2004], also exhibit strong diurnal cycles. In this case, the net convective transport of the chemical species from the boundary layer into the free troposphere will depend on the phase relationship between the diurnal cycle of the chemical tracer and the local rainfall rate.

The diurnal cycle in convective rainfall over land is poorly represented in many climate [Dai, 2006; Kim *et al.*, 2010; Yuan *et al.*, 2013] and weather forecast [Betts and Jakob, 2002; Clark *et al.*, 2007; Kim and Alexander, 2013; Kidd *et al.*, 2013] models. In many models, the diurnal rainfall peak occurs several hours too early and is often near local solar noon [Dai, 2006; Bechtold *et al.*, 2004]. This model bias in the diurnal timing of convective rainfall generates errors in the reflection of solar radiation back to space, especially by extensive upper tropospheric cirrus anvil clouds [Taylor, 2012] and is the dominant source of error in forecasts of tropical rainfall over land on short time scales [Chakraborty, 2010].

The convective available potential energy (CAPE) of an atmospheric column is usually calculated with respect to an air parcel originating from the surface. One can, however, vary the altitude of origin and calculate the CAPE of any air parcel in the boundary layer. The absorption of solar energy by the land surface increases the upward flux of heat and water vapor from the surface and increases the fraction of boundary layer air parcels with positive CAPE. The existence of near-surface air with positive CAPE is a thermodynamic precondition for moist convection. In many convective parameterizations, the convective cloud base mass flux is directly related to the CAPE of a single-model layer which is usually the model layer closest to the

surface [Grell, 1993; Jakob and Siebesma, 2003; Bechtold *et al.*, 2001]. However, there are many mechanisms which can delay the onset of convective precipitation. For example, it is likely that deep convective plumes entrain air not only from the shallow surface layer but also from the entire boundary layer. In this case, the mass-weighted CAPE of the boundary layer is likely to be a better proxy for the convective cloud base mass flux than the CAPE of the near-surface layer alone. We refer to the lag in the development of convective precipitation associated with the diurnal deepening of the near-surface convective layer as boundary layer resistance.

There are a variety of microphysical processes that also contribute to delays in the development of convective precipitation. These include delays associated with the formation of warm rain, and those associated with the time required for convective plumes to rise sufficiently high that the ambient temperature is cold enough to initiate the activation of ice condensation nuclei.

The entrainment of subsaturated air from the background atmosphere into convective plumes can also be expected to delay the onset of convective precipitation. Entrainment is associated with condensate evaporation, cooling, and loss of buoyancy. Due to mixing, most convective plumes dissipate before producing precipitation. However, by moistening the local atmosphere, they diminish the impact of entrainment on the development of subsequent plumes. There can therefore be an additional delay in the onset of deep convection, equal to the time scale over which shallow convection increases the midlevel relative humidity to the threshold required to support deep convection [Tompkins, 2001a; Guichard *et al.*, 2004].

Convective precipitation often occurs in association with some form of mesoscale organization such as squall lines [Tulich and Kiladis, 2012]. In this case, the development of convective precipitation can be expected to be delayed by processes associated with the development of the precipitating stratiform anvil, the formation of evaporatively driven downdrafts, and the horizontal propagation of the cold pools and gust fronts that provide the vertical uplift necessary to overcome convective inhibition and rapidly convert positive CAPE air near the surface into buoyant air within convective plumes.

Finally, at some locations, convection is associated with propagating convective systems that have been remotely generated by, for example, orography [Ahijevych *et al.*, 2004]. In this case, there would be an additional delay associated with the movement of convective systems from their place of origin.

Although there are numerous mechanisms which can delay the onset of convective rainfall over land, we show that the representation of the diurnal cycle in convective rainfall over land in a climate model can be significantly improved by a more accurate treatment of boundary layer resistance. Within each grid column, rather than restrict the initiation of convective updrafts to the model layer nearest the surface, we test for positive CAPE in each of the four lowest model layers. The parameterization could be easily modified to test for CAPE in higher model levels. However, positive CAPE above the first four levels was rare. The initial convective mass flux therefore responds to the convective instability of the column as a whole, rather than to the CAPE of a relatively thin layer near the surface. This modification delays the onset of convective rainfall over land and brings the diurnal rainfall peak into better agreement with observations.

The method outlined here for improving the diurnal cycle in convective rainfall over land is quite simple and should be relatively easy to implement in most climate models. There is, however, significant geographic variation in the amplitude and timing of the diurnal cycle in convective rainfall over land, especially in regions in which the convective rainfall appears to be affected by orography or coastlines. Our implementation of increased boundary layer resistance is therefore not able to generate realistic diurnal cycles in convective rainfall in all regions.

There have also been several recent attempts to improve the diurnal cycle in convective rainfall over land in climate models through the introduction of some form of subgrid-scale convective organization, irreversibility, or memory, into convective parameterizations. Convective organization can be introduced into convective parameterizations by using a variable from the local grid column from the previous or current time step to modify the behavior of the convective parameterization. Convective organization variables have included the height of the lifting condensation level [Stratton and Stirling, 2012], the existence of surface cold pools [Rio *et al.*, 2009], and column evaporation [Mapes and Neale, 2011]. These approaches tend to increase the initial resistance to the development of convective precipitation in a grid column, but once established, convective rainfall tends to be more persistent. The introduction of convective organization has had some success in delaying the onset of convective precipitation over land and generating more realistic

diurnal cycles [Rio *et al.*, 2009; Stratton and Stirling, 2012; Chao, 2013]. The convective parameterization used here implements a form of convective organization in which four of the parameters used in the convective scheme are an increasing function of the precipitation generated by the grid column over roughly the past 2 h. Our use of convective organization contributes to some of the improvement in the diurnal cycle in convective precipitation over land in our model.

The introduction of convective organization into convective parameterizations is intended to partially compensate for deficiencies that arise from the inability of climate models to represent subgrid-scale forms of convective organization that would otherwise persist across model time steps and have a strong effect on, for example, the cloud base mass flux. At higher spatial resolution, climate model simulations should be able to more naturally account for the inertia associated with the development of mesoscale convective systems and their persistence once established. However, while the diurnal cycle in convective rainfall over land does improve with increased resolution in some climate model simulations [Sato *et al.*, 2009; Ploshay and Lau, 2010; Yamada *et al.*, 2012], other simulations show little improvement [Yuan *et al.*, 2013]. The diurnal cycle is sometimes improved by the implementation of different convective parameterizations [Liang *et al.*, 2004]. Convective triggering schemes are in some ways similar to the introduction of convective organization and can also improve the diurnal cycle in convective rainfall [Zhang, 2003; Xie *et al.*, 2004; Lee *et al.*, 2008].

## 2. Overview of the Convective Parameterization

The model simulations discussed in this paper are based on an implementation of a recently developed convective parameterization [Folkens, 2009], referred to here as the IF parameterization, into version 4 of the Community Atmosphere Model (CAM4) [Neale *et al.*, 2013]. The climate model obtained by replacing the default schemes for both shallow [Hack, 1994] and deep [Zhang and McFarlane, 1995] convection with the IF parameterization in version 4 of the Community Atmosphere Model will be referred to as the CAM4-IF model.

The IF convective parameterization is a mass flux scheme in which the effects of convective updrafts and downdrafts on the background atmosphere are represented by a spectrum of updraft and downdraft parcels moving vertically under the influence of buoyancy. The updraft parcels originate from the four model levels closest to the surface. These levels occur at roughly 980, 958, 918, and 856 hPa, corresponding to pressure thicknesses of 14.5, 29.3, 53.0, and 72.7 hPa, respectively. At each of the four levels nearest the surface, we assume that subgrid-scale variability in temperature and relative humidity gives rise to an ensemble of updraft parcels with various values of moist enthalpy, as described in the Appendix A. Parcels from this spectrum with sufficient CAPE are given an initial upward kinetic energy, and subsequently move vertically using specified rules for precipitation formation and mass exchange with the background atmosphere. When the buoyancy of the parcel becomes negative, it fully detrains into the background atmosphere.

All condensate within updraft parcels is assumed to be liquid. Updraft parcels produce two kinds of precipitation. If the temperature of an updraft parcel is higher than  $T_{\text{freeze}}$  (here  $T_{\text{freeze}} = 270$  K), and the updraft parcel condensate loading exceeds a prescribed threshold, the excess condensate loading is converted to updraft rain. This form of precipitation is assumed to remain within the cloud at all heights, does not evaporate, and does not produce downdrafts. At temperatures colder than  $T_{\text{freeze}}$ , excess updraft parcel condensate is converted to updraft snow. This form of precipitation is assumed to remain within cloud until the melting level. At the first model level warmer than 0°C, this precipitation is assumed to exit cloud base, melt, start evaporating, and start generating downdrafts.

In the model, the induced grid-scale subsidence and heating within a convecting grid column tends to produce locally positive geopotential height anomalies with respect to neighboring columns. The outward pressure gradient accelerations associated with these geopotential height gradients will tend to produce divergent grid-scale outflows in the upper troposphere. The upward grid-scale motions required to balance this divergent upper tropospheric grid-scale outflow increase the relative humidity of the middle and upper troposphere. In this case, water vapor in excess of 90% relative humidity with respect to ice within any grid box above the melting level is converted to stratiform snow. This stratiform snow is then added to the updraft snow and treated in an identical manner.

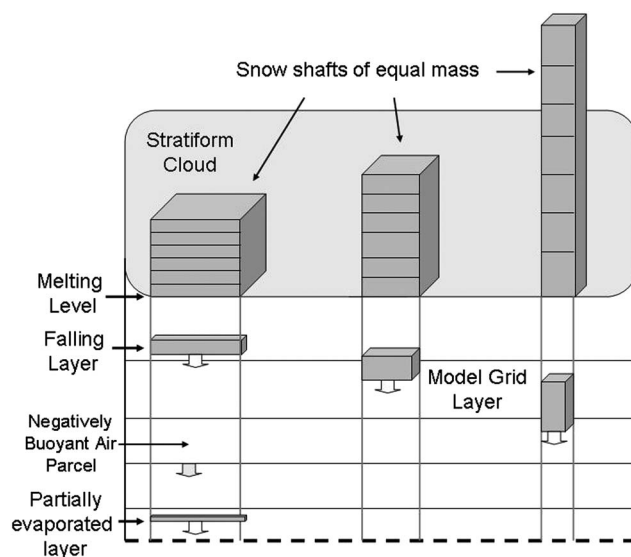


**Figure 1.** A conceptual diagram of the downdraft formalism of the convective parameterization. It is assumed that the base of precipitating stratiform clouds always occurs at the melting level. See the text for further details.

downdrafts. Within a convecting grid column, once the updraft parcel motions have been completed, the total snow flux from both updraft and stratiform sources is equally divided into three shafts. The three shafts are assigned lengths of 9 km, 20 km, and 45 km. The fraction of the grid column occupied by each shaft is calculated from the assumption that the local precipitation rate within each shaft is 100 mm/day, a representative rain rate for precipitating anvil clouds which are generating downdrafts [Leary and Houze, 1979]. Each snow shaft is divided into 15 layers. A descending snow layer encounters cloud-free air at the first model level having a temperature above 0°C. The snow layers of a snow shaft sequentially descend through the local grid column. In doing so they interact with air parcels at each model level whose fractional area is equal to the area of the parent snow shaft. These downdraft air parcels are effectively “entrained” from the grid column, and the snow parcels are considered to melt and evaporate within them as they fall toward the surface. The exposure time of a particular entrained air parcel to a snow/rain layer is determined in part from the remaining width of a snow/rain layer and its prescribed fall speed. In general, the negative buoyancy of an entrained air parcel will increase with the passage of every additional snow/rain layer through it. When the negative buoyancy of an air parcel is sufficiently large to overcome the stability of the atmosphere, the air parcel descends one model level. Due to interactions with multiple snow (rain) layers of a single snow shaft, an air parcel may descend multiple model levels within a time step and successively descend toward, and sometimes detrain at, the surface. This is more likely to occur for air parcels under the taller snow shafts, which have thicker snow (rain) layers, longer exposure times, and generate more intense cooling. The fall speed of the snow (rain) layers is parameterized in terms of temperature (as a surrogate for density) and typically decreases from 8 m/s just below the melting level to 5 m/s near the surface. No allowance is made for the slower fall speeds of snowflakes prior to melting. Each snow layer falls to the surface within a convective time step.

The moist enthalpy ( $k_m$ ), total water mixing ratio ( $r_t$ ), and dry mass ( $m_d$ ) of the updraft and downdraft parcels are updated as the parcels move vertically, mix, precipitate, and extract water from falling precipitation. Entrainment of updraft and downdraft parcels from the background atmosphere generates local sinks of  $k_m$ ,  $r_t$ , and  $m_d$ , whereas parcel detrainment generates sources of conserved quantities. It is assumed that the convective parameterization does not change the top and bottom pressure levels of each grid box and that the difference between the top and bottom pressure is related to the mass of a grid box via hydrostatic balance. At levels where the detrainment of mass exceeds entrainment, the grid box mass will exceed the hydrostatic mass (and conversely, where entrainment exceeds detrainment). To restore hydrostatic balance, the model moves mass vertically. For example, deep convection is typically associated with net mass detrainment at upper levels, and therefore triggers immediate downward subsidence within the grid column. Net upward vertical motion associated with the convective (subgrid-scale) movement of updraft and

In convective regions, the upper part of the boundary layer also tends to become supersaturated. Below 750 hPa, we remove moisture in excess of 90% relative humidity with a 2 h time scale. The rain generated by this stratiform mechanism is added to the updraft rain and treated in an identical manner.

The default CAM4 model has a parameterization for producing precipitation from the grid-scale condensate. This source of precipitation is turned off whenever the IF convective parameterization is activated. As a result, it has very little effect on the precipitation of convective regions and does not affect the results discussed in this paper.

Figure 1 gives a conceptual overview of the procedure used to generate

downdraft parcels is therefore usually associated with downward advection. This downward advection is usually associated with positive advection of dry static energy and negative advection of water vapor mixing ratio, generating heating and drying within the column.

Convective organization has been introduced into the IF convective parameterization by making four of the model parameters an increasing function of the local precipitation generated by the convective scheme over the past 2 h. These include (i) an AMP factor, which increases the cloud base mass flux, (ii) a  $dk_m$  parameter, which determines the width of the moist enthalpy updraft parcel spectrum, (iii) a  $f_{\text{deep}}$  parameter, which determines the fraction of updraft parcels which mix less rapidly with the background atmosphere, and (iv) a  $f_{\text{precip}}$  parameter, which determines the fraction of updraft condensate in excess of a prescribed threshold that is converted to precipitation. Increases in these parameters tend to favor the production of additional convective precipitation. Their introduction therefore tends to favor the nonlinear growth in convective precipitation and make convection less likely at low rain rates. These parameters are described in more detail in Appendix A.

Both the default CAM4 model and the CAM4-IF model with the new convective parameterization were run with a horizontal resolution of  $1.9^\circ \times 2.5^\circ$  (latitude  $\times$  longitude), 26 vertical levels, and a time step of 30 min. The model runs start on 1 January 2000 and end on 31 December 2002, using fixed climatological sea surface temperatures [Gent *et al.*, 2011]. The initial atmospheric state was a climatological state for the start date from the CAM4 model.

### 3. Data Sets

There is significant geographic variability in the diurnal cycle of convective rainfall over land [Yang and Slingo, 2001]. Here, we use the Tropical Rainfall Measuring Mission (TRMM) 3B42-gridded rainfall data set [Liu *et al.*, 2012] to determine the spatial variability in the monthly mean diurnal cycle of convective rainfall. This data set has a temporal resolution of 3 h and a spatial resolution of  $0.25^\circ$ . We use TRMM 3B42 rain rates from 2003 to 2010 to calculate the mean diurnal cycle in rainfall within every CAM4 grid cell. For each land grid cell in which the convective precipitation exceeds 2 mm/d, we calculate the correlation coefficient between the TRMM diurnal cycle and the diurnal cycles of various CAM4 model simulations. The global average of this correlation coefficient is then used as an indicator of the fidelity with which the model matches the observed diurnal cycle. We also use the TRMM 3B42 data set to assess the accuracy of the climatological rainfall patterns generated by the CAM4-IF model.

The climatological monthly mean longwave and shortwave top of the atmosphere fluxes of the CAM4 and CAM4-IF models are compared with data from the Clouds and the Earth's Radiant Energy System (CERES) Energy Balanced and Filled Top-of-Atmosphere Data Set [Wielicki *et al.*, 1996]. All-sky fluxes were available from March 2000 to June 2012 with a spatial resolution of  $1^\circ$ . The CERES data were spatially averaged to the CAM4 grid resolution for comparison with model output. We used edition 2.6 of the longwave data set and edition 2.7 of the shortwave data set. The CERES fluxes are best estimates obtained using a variety of satellite platforms and input data.

The monthly mean temperature and relative humidity profiles of the CAM4 and CAM4-IF models were compared with monthly mean profiles from the following 13 tropical radiosonde stations: Belize ( $17.53^\circ\text{N}$ ,  $271.70^\circ\text{E}$ ), Grand Cayman ( $19.3^\circ\text{N}$ ,  $278.63^\circ\text{E}$ ), Hilo ( $19.72^\circ\text{N}$ ,  $204.93^\circ\text{E}$ ), San Juan ( $18.43^\circ\text{N}$ ,  $294^\circ\text{E}$ ), Koror ( $7.33^\circ\text{N}$ ,  $134.48^\circ\text{E}$ ), Lihue ( $31.98^\circ\text{N}$ ,  $200.65^\circ\text{E}$ ), Majuro ( $7.08^\circ\text{N}$ ,  $171.38^\circ\text{E}$ ), Pago Pago ( $14.33^\circ\text{S}$ ,  $189.28^\circ\text{E}$ ), Ponape Island ( $6.97^\circ\text{N}$ ,  $158.22^\circ\text{E}$ ), Seawell ( $13.07^\circ\text{N}$ ,  $300.49^\circ\text{E}$ ), Truk ( $7.47^\circ\text{N}$ ,  $151.85^\circ\text{E}$ ), Yap Island ( $9.48^\circ\text{N}$ ,  $138.08^\circ\text{E}$ ), and Guam ( $13.55^\circ\text{N}$ ,  $144.83^\circ\text{E}$ ). The radiosonde data were downloaded from the United States High Resolution Radiosonde Data Archive archived at the Stratospheric Processes And their Role in Climate (SPARC) Data Center. At most stations, the twice daily profiles were available from 1998 to 2011.

### 4. Comparison With Observed Diurnal Cycle

Figure 2 shows the diurnal rainfall cycle simulated by the CAM4 and CAM4-IF model runs in four regions: the southeast United States, equatorial Brazil, equatorial Africa, and northern India. We also show the diurnal cycle from the TRMM 3B42-gridded rainfall data set. The boundaries of each region are shown in Figure 3b. We chose areas that had weak orography and selected months in which each region had enhanced rainfall. The rainfall of the CAM4 (default) model peaks near solar noon, a feature common to many climate

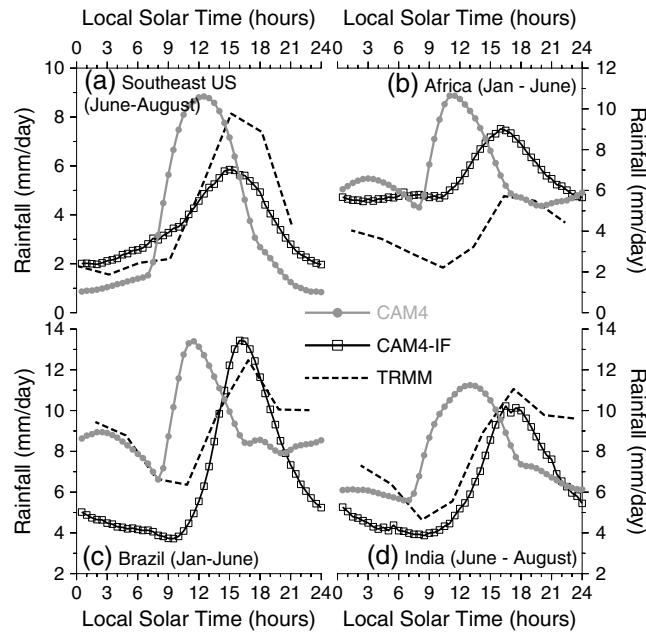


**Figure 2.** Each curve refers to the diurnal variation in rainfall of one of the four regions shown in Figure 3b. Dashed curve: TRMM 3B42. Gray curves with solid circles: default CAM4 model. Black curves with open boxes: CAM4-IF model.

monthly mean rain rates exceeded 2 mm/d and at locations where the rainfall could be assumed to be convective. Within the 20°S–20°N latitude range, rainfall was considered to be convective throughout the

models [Bechtold et al., 2004; Dai and Trenberth, 2004]. The CAM4-IF model simulates the timing of the late afternoon rainfall maximum in all four regions.

Figure 3b shows the geographic variation in the correlation coefficient between the CAM4-IF and TRMM diurnal cycles. The TRMM rainfall rates were first spatially averaged to the 1.9° × 2.5° horizontal resolution of the CAM4 model and then used to calculate the monthly mean diurnal variation at each grid cell. The 3 years of rainfall data from the CAM4-IF model run were used to determine the average rain rate at the eight daily TRMM times. We then calculated, for each month, the correlation coefficient between the eight local TRMM and CAM4-IF diurnal rain rates. This was done only at land grid cells where both the TRMM and CAM4-IF

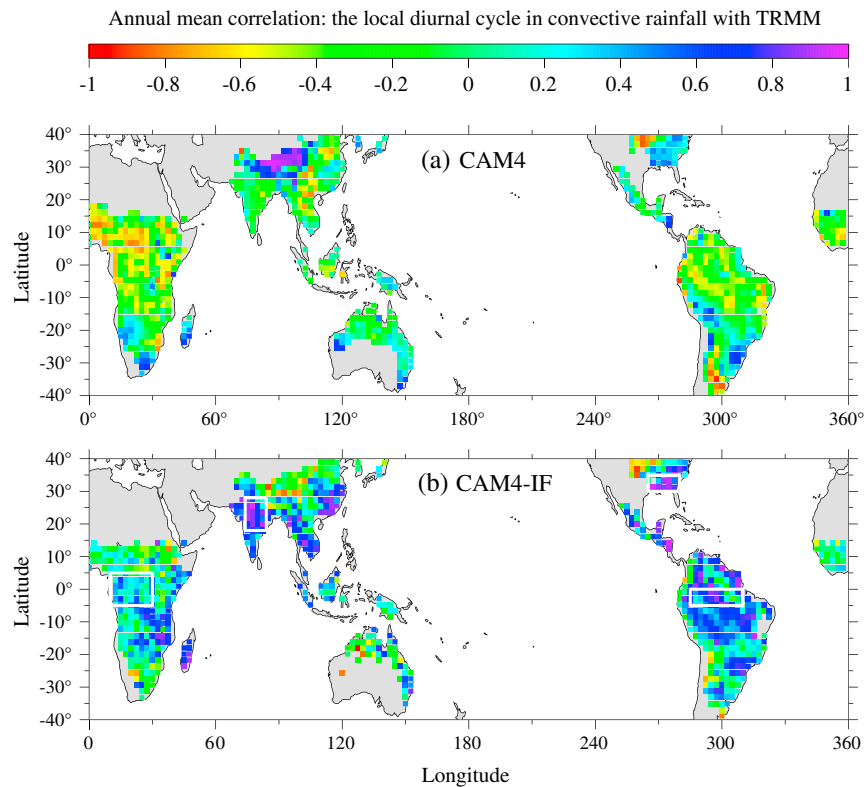


**Figure 3.** (a) The spatial variation in the annual mean correlation coefficient of the default CAM4 model with the local TRMM diurnal cycle. (b) The spatial variation in the annual mean correlation coefficient of the default CAM4-IF model with the local TRMM diurnal cycle. The rectangular regions outlined in white refer to the areas in Figure 2.

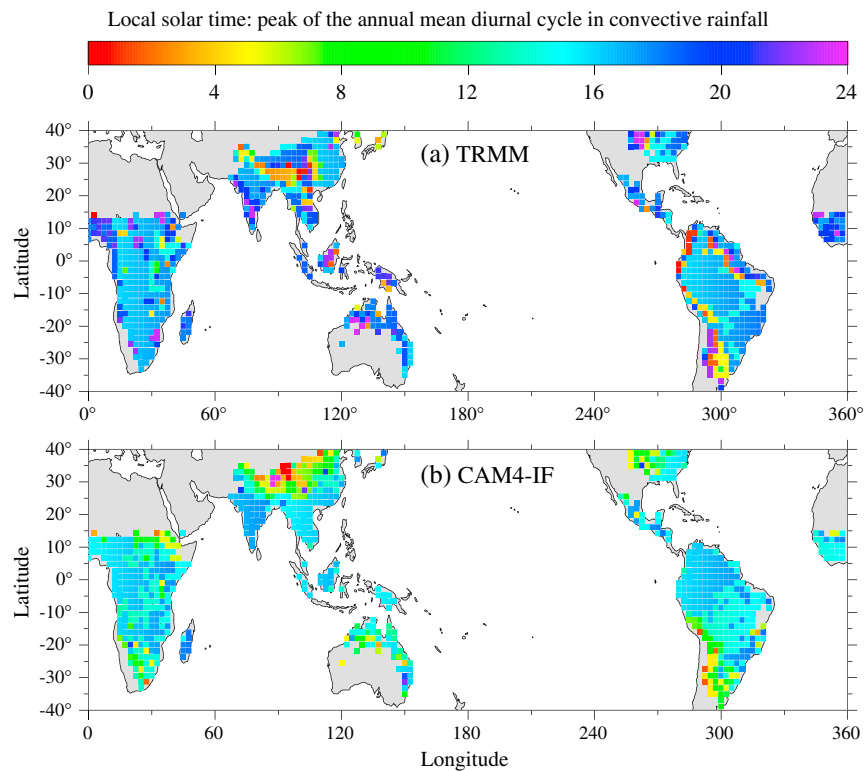


**Figure 4.** (a) The local solar time of the peak in the annual mean TRMM diurnal cycle. (b) The local solar time of the peak in the annual mean CAM4-IF diurnal cycle.

year. Within the 20°S–40°S and 20°N–40°N latitude windows, rainfall was considered to be convective during the December–February and June–August seasons, respectively. The correlation coefficients shown in Figure 3 were obtained by averaging over the months in which the above two conditions were satisfied. For an individual month, using the eight common diurnal data points available, the threshold for statistical significance at the 95% level is  $r = 0.62$ . This is achieved for 24% of the land grid cells. These cells are indicated in Figure 3b (blue and purple colors). This includes most of India, the southeast United States, Central America, and tropical South America. The diurnal cycle is poorly simulated in much of Africa, the interior of China, northern Australia, and the midwestern United States.

Figure 3a shows the spatial variation in the annual mean correlation coefficient between the default CAM4 and TRMM diurnal rainfall cycles, calculated using the same criteria as described above for the CAM4-IF model. The CAM4 model accurately simulates the diurnal cycle in only a few regions.

Figures 4a and 4b show the geographic variation in the local solar time of the TRMM and CAM4-IF diurnal rainfall peaks. The local time of peak rainfall was calculated from the annual mean diurnal cycle of convective rainfall. The months in which the local rain was considered to be convective were the same as defined earlier. The spatial variation in the time of the local TRMM rainfall peak is similar to maps shown previously, with a late afternoon or early evening peaks in most regions but with overnight rainfall peaks in locations such as the American midwest, the northeast coast of Brazil, and the interior of China [Yang and Slingo, 2001; Chao, 2013]. In general, Figure 4b tends to be a lighter shade of blue than Figure 4a, indicating that the diurnal rainfall peak of the CAM4-IF model tends to occur slightly earlier than the peak in TRMM rainfall. In general, the CAM4-IF model does not simulate the spatial variation in the timing of the local diurnal rainfall peak.

A comparison of Figures 3b and 4a suggests that the accuracy of the CAM4-IF simulation of the local diurnal cycle is compromised in regions where the local TRMM rainfall peak does not occur during the usual late afternoon to early evening time window. For example, Figure 4a exhibits three nearly parallel diagonal lines of anomalous rainfall timing in tropical South America, one of which corresponds to the Andes. Each of these diagonal lines is associated with a line of reduced correlation at a similar location in Figure 3b. Other

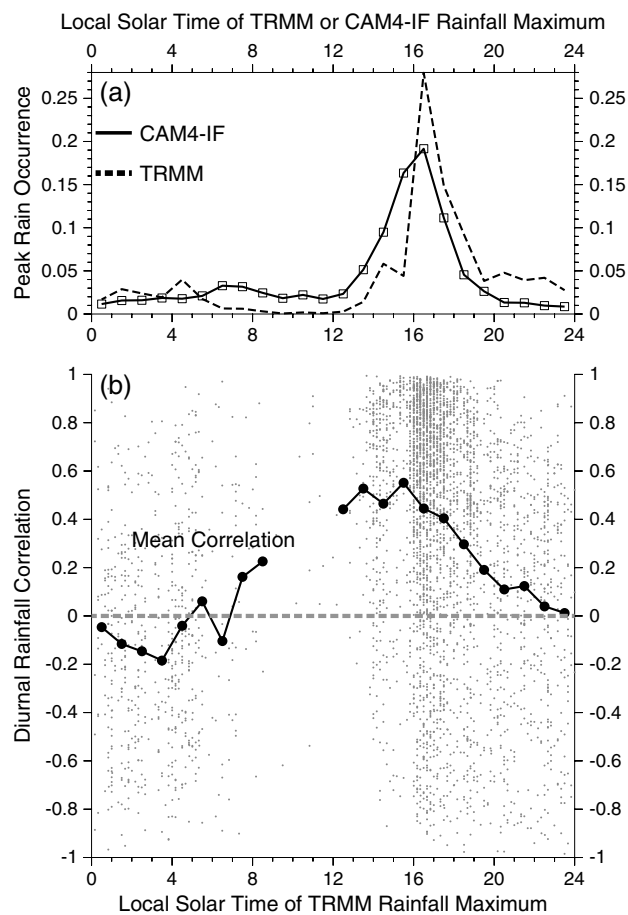


**Figure 5.** (a) Dashed curve: the frequency of occurrence of the local time of peak TRMM 3B42 rainfall, for convective land grid cells where the monthly mean rain rate exceeded 2 mm/d. Solid curve: the frequency of occurrence of the local time of peak rainfall from the CAM4-IF model. (b) The gray dots refer to the correlation coefficient between the CAM4-IF and TRMM diurnal cycles of a particular grid cell, plotted against the local time of peak TRMM rainfall. The solid curve was obtained by binning the correlation coefficients in 1 h increments.

complexes [Velasco and Fritsch, 1987; Salio et al., 2007]. It can be expected that many of these features would be difficult to simulate in coarse resolution climate models. However, some of the regional variation in the diurnal cycle of South American convective rainfall has been simulated by a regional-scale model with 50 km resolution [da Rocha et al., 2009]. Over the United States, there was a mixed improvement in the simulation of the diurnal cycle when the horizontal grid size was decreased from 2° to 0.5° [Lee et al., 2007].

In Figure 5b, we show how the correlation between the CAM4-IF and TRMM diurnal cycles in convective rainfall varies with the local solar time of the TRMM diurnal rainfall peak. The individual points refer to the correlation coefficient of a grid cell for a particular month, while the solid line shows the mean dependence of the correlation coefficient on the local time of the TRMM rainfall peak. On average, the correlation coefficient is largest when the observed TRMM rainfall peak occurs between 13:00 and 18:00 local time. Figure 5a (dashed line) is a probability distribution function (PDF) of the local solar time of the TRMM diurnal rainfall peak, constructed from grid cells at which the local rainfall could be considered to be convective using the previous definition, and at which the monthly mean rain rate exceeded 2 mm/d. The most probable time for the TRMM diurnal rainfall peak is 16:30 in the late afternoon. The solid curve of Figure 5a shows the PDF of the local solar time of the diurnal rainfall peak from the CAM4-IF model. Although the overall shape of the CAM4-IF PDF is similar to the TRMM PDF, the CAM4-IF maximum occurs slightly earlier than the TRMM maximum, and the CAM4-IF PDF under represents the frequency of occurrence of rainfall peaks during the night.

regions of anomalous rainfall timing, and also low correlation, include northern Argentina, the American midwest, and the interior of China.

Some of the regional anomalies in the diurnal timing of convective rainfall shown in Figure 4a have been attributed to local changes in the genesis, propagation, or organization of convective systems. For example, the nighttime peak over the Great Plains of the United States has been attributed to the eastward propagation of mesoscale convective systems originating during the afternoon over the Rocky Mountains [Dai et al., 1999; Ahijevych et al., 2004]. Along the northeast coast of Brazil, the nocturnal maximum during the January to April time period has been attributed to a convergence zone forming near the coast between the onshore northeasterly trade winds and an offshore land breeze, with squall lines form along the convergence zone often propagating inland [Kousky, 1980; Cohen et al., 1995]. The middle diagonal line of maximum nighttime rainfall across Brazil appears similar to a feature that was previously tentatively attributed to a remote response to diurnally forced convection over the Andes [Garreaud and Wallace, 1997]. The region of anomalous diurnal timing in northern Argentina and Paraguay corresponds to a preferred region for the development of mesoscale convective

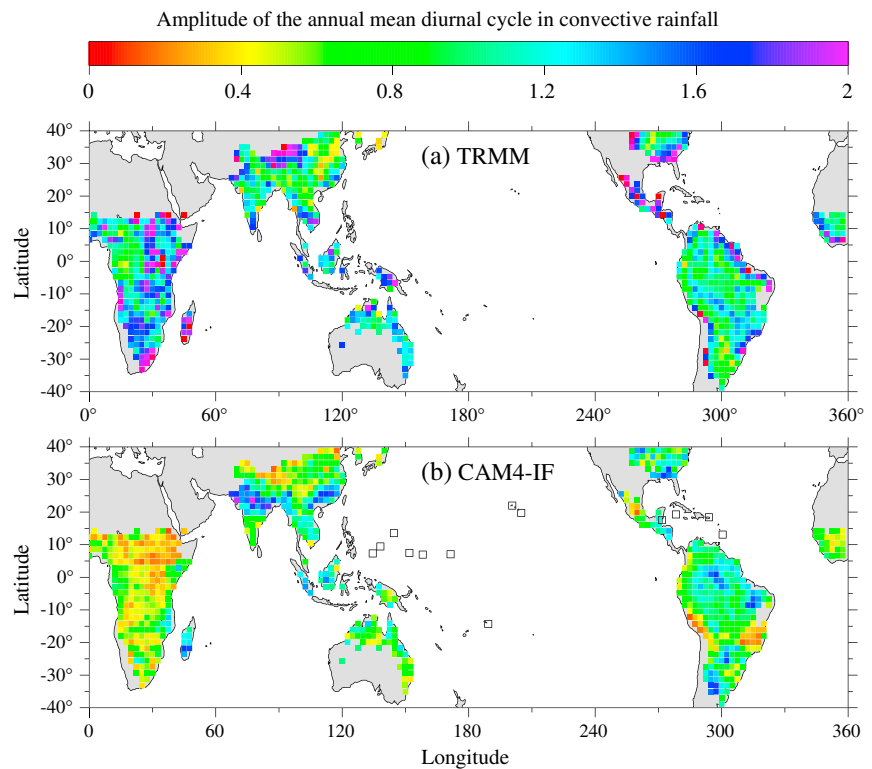


**Figure 6.** (a) The amplitude of the annual mean TRMM diurnal rainfall cycle. (b) The amplitude of the annual mean TRMM diurnal rainfall cycle. The diurnal amplitude has been defined as the difference between the maximum and minimum rainfall rates, divided by the mean daily rainfall. The locations of the 13 tropical NOAA/National Climatic Data Center radiosondes used here have been identified using open boxes.

Figures 6a and 6b show the regional variation in the amplitude of the annual mean TRMM and CAM4-IF convective rainfall diurnal cycles, with the annual mean again constructed using the previous definition of months considered convective. The diurnal amplitude was defined as  $(R_{max} - R_{min})/R_{mean}$ , where  $R_{max}$ ,  $R_{min}$ , and  $R_{mean}$  refer to the maximum, minimum, and mean rainfall rates using the eight rain rates used to define the local diurnal cycle. Although defined somewhat differently, the spatial variation in the amplitude of the TRMM diurnal cycle is similar to previous maps [Yang and Slingo, 2001; Chao, 2013] of the observed diurnal cycle, with amplitude maxima over the northeast coast of Brazil, Central America, the southeast United States, and parts of Africa. In general, the CAM4-IF model is not able to simulate the spatial variability in the amplitude of the TRMM diurnal cycle. In the CAM4-IF model, for example, the amplitude of the diurnal cycle in East Africa is near zero, whereas the TRMM amplitude is quite large.

### 5. Effect of the Mass Flux Closure

It is not possible to isolate a single reason for the improvement in the diurnal cycle of convective rainfall in going from the default CAM4 model to the CAM4-IF model. However, much of the improvement results from a change in the mass flux closure. Prior to deep convection, the default CAM4 model first identifies the layer near the surface with the largest moist static energy. This is usually the layer closest to the surface. If the CAPE of an air parcel launched from this layer exceeds a threshold of 70 J/kg, mass is removed from the layer with a 1 h time scale and entrained into a convective plume which subsequently rises within the grid column. The CAM4-IF model, on the other hand, calculates the CAPE of the bottom four model layers. If the CAPE of any layer exceeds a threshold of 100 J/kg, mass from the layer is used to construct an updraft parcel spectrum as described in Appendix A. In this method, the total initial updraft parcel mass roughly scales with the CAPE of the boundary layer as a whole, rather than the CAPE of a relatively thin layer near the surface. This difference can affect the diurnal variation in convective rainfall generated by the two models. Figure 7 shows the diurnal variation in the CAPE of the near-surface layer of the CAM4-IF model, and of the

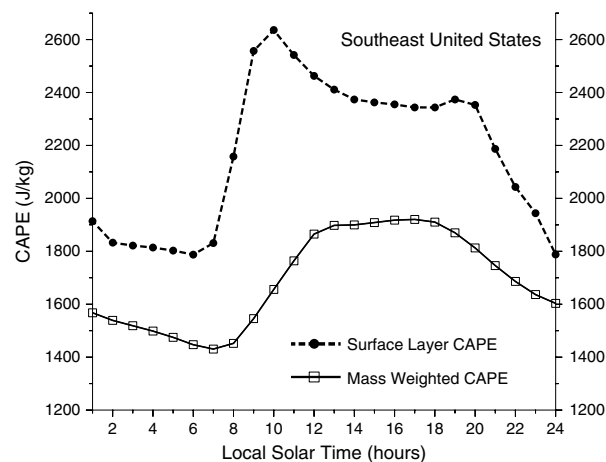


**Figure 7.** Dashed line: the diurnal variation of the CAPE of the lowest model layer. Solid line: The diurnal variation of the mass-weighted CAPE of the four lowest model layers. Both curves were obtained from the CAM4-IF model from the southeast United States region during July.

convective rainfall, we ran three additional simulations of the CAM4-IF model. In the LEV1, LEV2, and LEV3 simulations, updraft parcels were entrained from only the lowest one, two, and three model levels, respectively. As described in the Appendix A, the cloud base mass flux of each model layer is proportional to the CAPE of that layer. If the number of model levels from which updraft parcels may originate is reduced, the convective mass flux will be reduced and convection will tend to occur at larger and less realistic values of CAPE. To compensate for the reduction in the number of levels from which updraft parcels may originate, the convective removal time scale  $t_{\text{remove}}$  in the three simulations was reduced to 2 (LEV1), 4 (LEV2), and 8 (LEV3) h.

We also wanted to investigate the degree to which the implementation of subgrid-scale organization was affecting the simulation of the diurnal cycle. We therefore ran two additional simulations. In the NO-ORG simulation, all four organization variables were fixed at constant values. This includes (with the fixed value in brackets) the mass flux amplification factor AMP (3), the updraft parcel spectrum width  $dk_m$  (0 J/kg), the deep mixing fraction  $f_{\text{deep}}$  (0.50), and the updraft condensate to precipitation conversion efficiency  $f_{\text{precip}}$  (0.5). In a second simulation called NO-AMP, the mass flux amplification factor was fixed as given above, but the other three organization parameters varied as described in Appendix A.

For each of the five additional simulations, we calculated the global mean correlation coefficient between the TRMM and simulated diurnal cycles in the same manner as described earlier. The variation in the global mean correlation between the model runs is shown in Figure 8. The solid curve refers to the value of the correlation over land, while the dotted curve shows the correlation over the ocean. Over land, the default CAM4 model had the lowest value global mean correlation, with an overall anticorrelation with the TRMM diurnal cycle. For the CAM4-IF model, there was a progressive improvement in the simulation of the diurnal cycle as additional near-surface layers were permitted to generate convective updraft parcels. The addition of subgrid-scale convective organization was also associated with an improvement in the simulation of the diurnal cycle, with the average correlation coefficient of the CAM4-IF model run higher than the coefficients of both the NO-AMP and NO-ORG model runs. Over the ocean, the correlation coefficients of the six model runs were similar to each other, with the default CAM4 model exhibiting a slightly higher correlation than the other five model runs.

## 6. Comparison With Other Observations

New implementations of convective parameterizations in climate models are tested against a large number of metrics in addition to the diurnal cycle. It is desirable that increased agreement in one metric not be offset by decreased agreement in others. Although the comparisons given here are not intended to be definitive, it is our experience that allowing convective updraft parcels to originate from the lowest four model layers (as opposed to just the near-surface layer) does not undermine other aspects of the CAM4-IF model.

average mass-weighted CAPE of the lowest four model layers, both averaged over the southeast United States region in July. The boundary layer CAPE was calculated by using each of the four lowest layers as a launch level and then weighting the resulting CAPE of each layer by the appropriate pressure thickness. The CAPE of the near-surface layer sharply increases after sunrise and peaks near 10:00 [Chao, 2013]. The secondary peak near 20:00 is caused by an early evening local increase in near-surface water vapor mass mixing ratio. However, the mass-weighted CAPE of the boundary layer responds much more slowly to the morning increase in solar insolation and reaches a weak maximum near 16:00.

To investigate the effect of changes in the mass flux closure on the diurnal cycle of

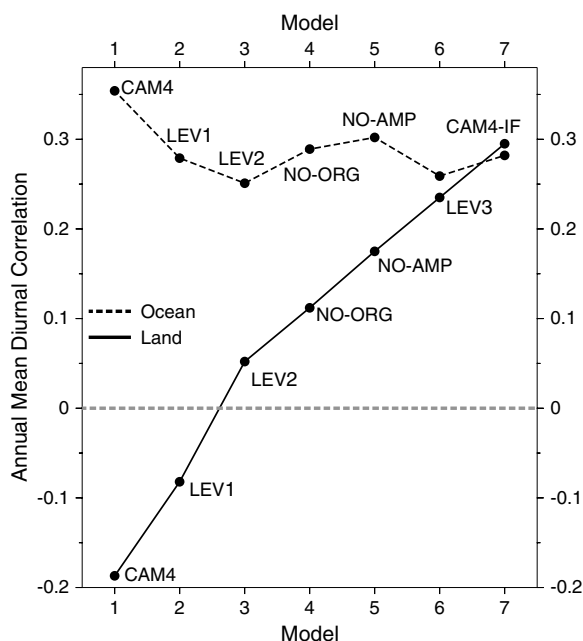


**Figure 8.** The annual mean correlation between the simulated and TRMM diurnal rainfall cycles, plotted as a function of model simulation. The solid curve refers to the correlation coefficient obtained from convective locations over land, while the dashed curve refers to convective locations over the ocean. The horizontal axis refers to different model simulations. Model 1 refers to the default CAM4 model. Model 7 refers to the CAM4-IF model. The remaining points refer to modifications of the CAM4-IF model.

definitions of the two axes, the distance of a particular model point from the REF point on the x axis in Figure 9 becomes proportional to the centered root-mean-square (RMS) difference between the simulated and observed rainfall patterns. The CAM4-IF results are shown in Figure 9 (solid circles), while the default CAM4 results are shown in Figure 9 (open squares). In the case of ocean rain (Figure 9, label 1), the CAM4-IF model has a much larger normalized standard deviation than the CAM4 model, and therefore has a much larger RMS difference. In the case of land rain (Figure 9, label 2), the CAM4 model has a smaller normalized standard deviation and a smaller RMS difference.

The rainfall climatology obtained from the 2003–2010 TRMM rainfall rates is an average over changes in rainfall due to both internal atmospheric variability and changes in sea surface temperatures. The model runs were conducted using fixed sea surface temperatures, and as such, only include variability that is internally generated by the atmosphere during a 3 year period. It would therefore not be anticipated that the RMS difference of the modeled rainfall fields from the TRMM rainfall fields would be zero, even in a “perfect” model.

**6.2. Shortwave and Longwave Fluxes**

The Taylor diagram shown in Figure 9 also shows the correlation coefficients and standard deviations of the top of the atmosphere 20°S–20°N shortwave and longwave fluxes of the two models. The CERES data set was used as the reference climatology. For both fluxes, the RMS difference of the CAM4-IF model is smaller than the RMS difference of the default CAM4 model.

It should be noted that some of the biases present in the representation of clouds in the CAM4 model have been diminished or resolved in the more recent CAM5 model [Kay et al., 2012]. Within an area similar to the southeast United States region shown in Figure 3b, the CAM5 model also appears to simulate the diurnal cycle in convective rainfall more accurately than the CAM4 simulation shown in Figure 2a.

**6.3. Temperature and Relative Humidity Profiles**

Figure 10a shows the temperature biases of the CAM4 and CAM4-IF models as a function of height, with respect to an annual mean tropical radiosonde profile. This profile was generated by the SPARC radiosonde

**6.1. Comparisons With Monthly Mean Rainfall**

The rainfall climatologies of the 3 year model runs were compared with the 2003–2010 TRMM rainfall climatology using a Taylor diagram [Taylor, 2001]. In this diagram, shown in Figure 9, the angular coordinate refers to the correlation coefficient between the modeled and TRMM monthly mean rain rates. In calculating the correlation, we restricted attention to grid cells and months for which the rain could be considered convective using the previous definition, and considered land and ocean regions separately. The radial coordinate refers to the standard deviation of the monthly mean convective rainfall rates of a model run (land and ocean again considered separately), normalized by the standard deviation of the TRMM monthly mean rain rates. Within each sum we used an appropriate area weighting factor, and the monthly rain rates were defined as an anomaly with respect to the annual global convective mean. With these

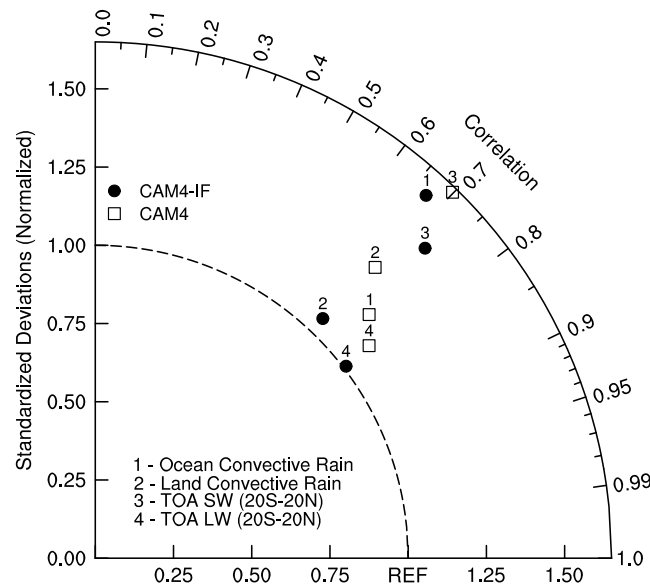


**Figure 9.** A Taylor diagram comparison of the CAM4-IF model (solid circles) with the default CAM4 model (boxes). The variables plotted are (1) ocean convective rain; (2) land convective rain; (3) top of the atmosphere-reflected solar radiation (20°S–20°N); (4) top of the atmosphere-reflected longwave radiation (20°S–20°N). The distance of a model variable from the REF location on the x axis corresponds to the centered root-mean-square (RMS) difference, in the case of the two rain variables, with a TRMM climatology, and in the case of the two radiative fluxes, with a CERES climatology.

stations indicated in Figure 6b (open squares). The temperature profiles of the models were averaged over the grid columns containing the radiosonde stations. The CAM4-IF model runs exhibit a cold bias throughout the troposphere that peaks in the upper troposphere. The default CAM4 model also has a cold bias in the upper troposphere and a small warm bias which peaks near 7 km. Figure 10b compares the relative humidity profiles of the models with an annual mean relative humidity profile obtained from the 13 radiosonde stations. Both models are quite successful in simulating the annual mean relative humidity profile in the lower troposphere (below 5 km). The CAM4-IF model exhibits a moist bias in the middle and upper troposphere. The CAM4 model has a smaller relative humidity bias in the middle troposphere but a larger relative humidity bias in the upper troposphere. The actual magnitude of the upper tropospheric moist bias of the models is unclear, however, as radiosondes tend to exhibit a dry bias at the colder temperatures characteristic of the upper troposphere [Kley et al., 2000]. Though obtained from a restricted set of radiosonde stations, the temperature and relative humidity biases of the CAM4 model shown in Figure 10 are similar

characteristic of the upper troposphere [Kley et al., 2000]. Though obtained from a restricted set of radiosonde stations, the temperature and relative humidity biases of the CAM4 model shown in Figure 10 are similar

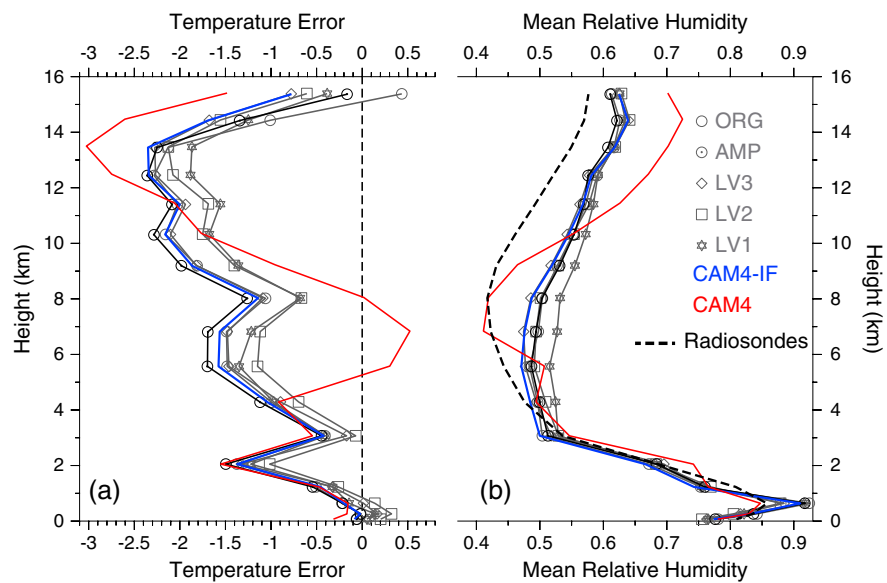


**Figure 10.** (a) The temperature bias of the models with respect to an annual mean tropical radiosonde climatology. The default CAM4 model is shown in red, while the CAM4-IF model is shown in blue. The gray curves refer to various modifications of the CAM4-IF model. (b) The dashed curve refers to an annual mean tropical relative humidity climatology. At temperatures colder than 0°C, the relative humidity has been calculated with respect to the saturated vapor pressure of ice. The annual temperature and relative humidity profiles were obtained from the 13 radiosonde stations shown in Figure 6b.

to the overall tropical biases of the CAM4 model previously calculated with respect to a reanalysis data set [Neale *et al.*, 2013].

## 7. Summary

Most of the convective parameterizations used in climate models are mass flux-based parameterizations in which the effects of convective clouds on the background atmosphere are represented by updraft plumes or parcels moving upward under the influence of buoyancy. In many convective parameterizations, the updraft plume or parcel is entrained from the model level with the highest moist static energy or a relatively thin surface layer [Grell, 1993; Jakob and Siebesma, 2003; Bechtold *et al.*, 2001]. However, there is no reason, other than computational expediency, to restrict the initiation of convective clouds exclusively to a single layer near the surface. Over the tropical oceans, the positive CAPE surface layer typically extends to 900 hPa, while over southeast United States, the positive CAPE layer typically extends to 800 hPa [Mitovski and Folkins, 2013]. In the default CAM4 model, due to the practice of restricting the initiation of convective plumes to the layer with highest moist static energy, convective plumes usually originate from a near-surface layer that has a pressure thickness of about 14.5 hPa. In this case, in order to generate realistic deep convective mass fluxes, it is necessary that the convective removal time scale from this layer be very short (1 h).

The rapid removal of positive CAPE air from a thin surface layer generates a bias in the simulation of the diurnal cycle. Over land during the day, boundary layer turbulence gives rise to an upward flux of heat and water vapor from the Earth's surface. This upward transport helps generate air parcels with positive CAPE throughout the boundary layer. Because of the time lags associated with this upward transport, the mass-weighted CAPE of the boundary layer responds more slowly to increases in solar insolation than the CAPE of the surface layer. Climate models should therefore be able to improve their representation of the diurnal cycle in convective rainfall over land by using convective parameterizations which employ mass flux closures which are sensitive to the convective instability of the grid column as a whole, rather than a thin surface layer. We have shown that the CAM4-IF model exhibits a significant improvement in the simulation of the diurnal cycle in convective rainfall over land as the number of near-surface levels used to generate convective air parcels increases from one to four. As a result, the CAM4-IF model is able to simulate the diurnal cycles in convective rainfall over land and ocean to a comparable accuracy.

The method outlined here for generating the late afternoon peak in convective rainfall over land is quite simple and seems to be the most natural explanation from an energetic point of view. However, within the boundary layer, moist static energy usually decreases with height. If updraft air parcels are initially entrained from a larger number of near-surface model layers, the average initial updraft moist static energy will decrease. As a result, it may be necessary to modify the mixing schemes of convective parameterizations in order to retain a strong outflow mode in the upper troposphere.

In addition to boundary layer resistance, it is likely that there are numerous other physical mechanisms that can affect the timing of the diurnal peak in convective rainfall. In particular, some of the improvement in the diurnal cycle of convective rainfall in the CAM4-IF model comes from the implementation of convective organizational variables or convective memory, as reported by other authors [Rio *et al.*, 2009; Stratton and Stirling, 2012; Chao, 2013].

For the most part, our implementation of convective organization is not able to simulate the diurnal cycle in regions where the diurnal peak in convective rainfall occurs at night. Most of the rainfall in these regions appears to be associated with organized convective systems that are either remotely generated, or associated with local synoptic forcings that favor nighttime development. In these regions, the correlation between the local diurnal cycle simulated by the CAM4-IF model and the observed diurnal cycle measured by TRMM is only weakly positive. Significant further improvement in the simulation of the diurnal cycle in convective rainfall over land by the CAM4-IF model will therefore probably require more realistic simulations of the types of convective organization that generate peak rainfall rates during the evening.

## Appendix A: Subgrid-Scale Convective Organization in the CAM4-IF Model

The one-dimensional behavior of the IF convective parameterization has been described previously [Folkins, 2009]. During implementation into the CAM4 model, the parameterization was modified to include a form of subgrid-scale organization. Rather than being fixed at constant values, four of the model parameters

depend on the mean precipitation rate generated by the model grid column over the past 2 h. Although the improvement in the simulation of the diurnal cycle in convective rainfall associated with the introduction of convective organization is modest, its introduction does have a number of important benefits. It gives rise to more rapid rates of growth and decay of convective precipitation, an increase in the mean height of divergent outflow from shallow to deep during the development of high rain events, and a boundary layer cooling that is coincident with high rain rates. The next four sections give a more detailed discussion of convective organization in the IF convective parameterization.

### A1. Boundary Layer Moist Enthalpy Spectrum

When convective precipitation is present, there is an increase in the variability of boundary layer temperature and specific humidity [Zhang and Klein, 2010]. Cloud-resolving model simulations show that, during convection, the moist static energy of parcels recently heated by the surface can exceed the moist static energy of boundary layer downdraft parcels by as much as 10 kJ/kg [Khairoutdinov and Randall, 2006]. The updraft parcels that originate from each of the four model levels closest to the surface are therefore assigned a range of moist enthalpy values. Let  $k_m$  refer to the moist enthalpy of a grid box,  $N$  to the number of updraft parcels in the moist enthalpy updraft parcel spectrum, and  $dk_m$  to the width of the spectrum. The initial moist enthalpy of updraft parcel  $i$  is then defined as

$$k_{m,i} = k_m + \frac{(i-1)}{(N-1)} dk_m, \quad (\text{A1})$$

with  $i$  ranging from 1 to  $N$ . Each parcel within the updraft spectrum of a grid box is assumed to have the same initial mass per unit area.

The width  $dk_m$  of the initial updraft parcel spectrum is an increasing function of the mean local rain rate  $R_{\text{mean}}$ , where  $R_{\text{mean}}$  is defined as

$$R_{\text{mean}} = \left(1 - \frac{t_{\text{step}}}{\tau_{\text{org}}}\right) R_{\text{mean,prev}} + \frac{t_{\text{step}}}{\tau_{\text{org}}} R_{\text{current}}. \quad (\text{A2})$$

The  $t_{\text{step}}$  refers to the time step of the CAM4 model (30 min),  $\tau_{\text{org}}$  is a time scale over which  $R_{\text{mean}}$  responds to changes in precipitation ( $\tau_{\text{org}} = 2$  h),  $R_{\text{mean,prev}}$  is the previous local value of the mean precipitation rate, and  $R_{\text{current}}$  is the current precipitation rate in the grid column. With this definition,  $R_{\text{mean}}$  is roughly equal to the mean precipitation rate of the local grid column over the time interval  $\tau_{\text{org}}$ . It would be possible to simply set  $R_{\text{mean}}$  equal to the precipitation at the most recent time step by using  $\tau_{\text{org}} = t_{\text{step}}$ . However, this tends to introduce excessive nonlinearity into the rainfall rate generated by the model. The values of the convective organization variables therefore respond in a slightly lagged manner to changes in local rainfall.

The width  $dk_m$  of the moist enthalpy spectrum is then defined using the following sigmoidal expression.

$$dk_m = dk_{m,\text{min}} + \frac{dk_{m,\text{max}}}{1 + e^{-R_{\text{norm}}}} \quad (\text{A3})$$

Minimum width of the enthalpy spectrum is  $dk_{m,\text{min}}$ ,  $dk_{m,\text{min}} + dk_{m,\text{max}}$  is the maximum width, and  $R_{\text{norm}}$  is defined in terms of  $R_{\text{mean}}$  and two additional rainfall parameters  $R_{\text{half}}$  and  $R_{\text{scale}}$ .

$$R_{\text{norm}} = \frac{R_{\text{mean}} - R_{\text{half}}}{R_{\text{scale}}} \quad (\text{A4})$$

$R_{\text{half}}$  is the rain rate at which the spectrum width is roughly equal to half its maximum value.  $R_{\text{scale}}$  is a parameter that determines the steepness of the sigmoidal curve. For small  $R_{\text{scale}}$ , the sigmoidal function approaches a step function. Figure A1 shows the dependence of  $dk_m$  on  $R_{\text{mean}}$  obtained by using the above three equations, and the parameter values given in Table A1.

If the convective precipitation within a grid column increases, the sigmoidal expression for  $dk_m$  will increase the value of  $dk_m$  parameter on the next time step. This increase in boundary layer variance will tend to increase the fraction of the boundary layer mass with positive CAPE and contribute to a further increase in convective precipitation. The introduction of the  $dk_m$  parameter therefore contributes to a nonlinear intensification of high rain events and an increase in the overall rainfall variance. The downdraft formulation of the model is constructed to enable the direct injection of downdraft parcels with reduced moist static energy into the boundary layer. Without the introduction of a moist enthalpy spectrum, this direct injection of cold

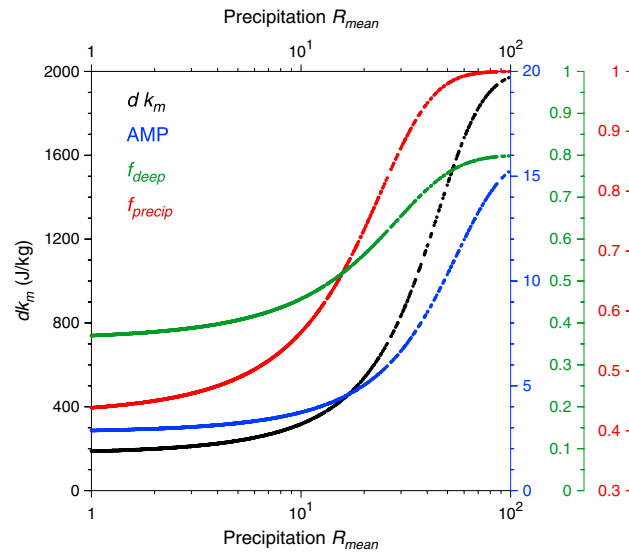


**Figure A1.** Each curve shows the sensitivity of a particular variable used in the convective parameterization to  $R_{mean}$ , roughly equal to the mean rainfall rate of a grid column over the previous 2 h. The formulas used to calculate the sigmoidal curves are given in Appendix A. At low values of  $R_{mean}$ , the variables converge to the minimum value listed in Table A1. At large values of  $R_{mean}$ , the variables converge toward the sum of the minimum and maximum values listed in Table A1.

Apart from defining an updraft parcel spectrum at each initial starting level, the above expression is similar to the mass flux closures used in other convective parameterizations. Convection occurs in response to the presence of CAPE. However, we have introduced an additional parameter AMP. This parameter depends on the lagged mean rainfall rate  $R_{mean}$  in the same way that the  $dk_m$  parameter depends on  $R_{mean}$ , except that we use different coefficients. These coefficients are given in Table A1. The resulting dependence of AMP on  $R_{mean}$  is shown in Figure A1. The introduction of this parameter also tends to generate faster growth rates of convective rainfall.

### A3. Deep- and Shallow-Mixing Fractions

Within the initial updraft parcel spectrum of a model layer, parcels whose CAPE exceeds 100 J/kg are given an initial upward kinetic energy of 20 J/kg to overcome the local convective inhibition. This is a virtual kinetic energy which is not exchanged with the energy of the column. At each subsequent model level, air parcels mix with the background atmosphere using a buoyancy gradient formalism in which the fractional mass entrainment (or detrainment) of a parcel at layer  $i$  is given by

$$\sigma = \frac{b_p(i + 1) - b_p(i - 1)}{b_{mix}}, \tag{A6}$$

where  $b_p(i - 1)$  is the buoyancy of the updraft parcel at the previous level and  $b_p(i + 1)$  is the buoyancy the parcel would have at level  $i + 1$ . The rate at which an updraft parcel mixes with the background atmosphere is inversely proportional to a buoyancy scale parameter  $b_{mix}$ . This formalism ensures that updraft

air would be a strong negative feedback on the development of high rain events in the model. The  $dk_m$  parameter can be tuned to generate a reasonable magnitude for the observed boundary layer cooling coincident with strong convective events [Mitovski and Folkins, 2013].

### A2. Cloud Base Mass Flux

At each of the four lowest model levels, we define an initial updraft parcel mass per unit area spectrum  $m_{p,i}$  (where  $i$  ranges from 1 to  $N$ ) using the following expression.

$$m_{p,i} = AMP \left( \frac{t_{step}}{t_{remove}} \right) \left( \frac{cape(i)}{cape_{scale}} \right) \left( \frac{dp}{gN} \right) \tag{A5}$$

The  $dp$  refers to the pressure difference between the top and bottom of a grid box,  $cape(i)$  to the CAPE of parcel  $i$  within the moist enthalpy updraft spectrum,  $cape_{scale}$  to a CAPE scale (800 J/kg),  $t_{remove}$  to a removal time scale (12 h).

**Table A1.** Parameter Values for the Variables Which are Assumed to Depend on the Local Degree of Convective Organization<sup>a</sup>

Variable	$R_{scale}$	$R_{half}$	Min Value	Max Value	Description
AMP	20 mm/d	40 mm/d	1	15	parcel mass amplification factor
$dk_m$	15 mm/d	35 mm/d	0 J/kg	2000 J/kg	parcel enthalpy spectrum width
$f_{deep}$	14 mm/d	14 mm/d	0.20	0.60	weak mixing fraction
$f_{precip}$	10 mm/d	15 mm/d	0.3	0.7	condensate precipitation fraction

<sup>a</sup>For each variable, the four parameters listed here are used to calculate a sigmoidal value of the variable using equations (A1) and (A2).

parcels entrain ( $\sigma > 0$ ) when their buoyancy increases with height, and detrain ( $\sigma < 0$ ) when their buoyancy decreases with height. Air parcels fully detrain into the background atmosphere at the first level at which their buoyancy becomes negative and they have exhausted their initial kinetic energy.

Visual images of convective clouds indicate that convective parameterizations should be able to simultaneously generate different types of convective activity within a grid column. In the IF parameterization, the initial moist enthalpy of an air parcel will depend on its level of origin and its position within the updraft parcel spectrum of that level. However, this initial moist enthalpy variability is not able to generate by itself a large range of convective outflow altitudes within a single grid column. We therefore introduce a second source of convective variability in which parcels with larger initial moist enthalpy experience within the updraft parcel spectrum of a layer experience reduced mixing by virtue of having a smaller  $b_{\text{mix}}$  value. Let  $i$  refer to the index of an updraft parcel within a spectrum. Its mixing parameter is then given by

$$b_{\text{mix}} = b_{\text{mix},0} + \frac{(i-1)}{(N-1)} \Delta b_{\text{mix}}.$$

Here,  $N = 5$  as specified above,  $\Delta b_{\text{mix}} = 0.06 \text{ m/s}^2$ , and  $b_{\text{mix},0}$  assumes two values. The updraft parcels with  $b_{\text{mix},0} = 0.20 \text{ m/s}^2$  usually detrain in the lower troposphere, while the updraft parcels with  $b_{\text{mix},0} = 0.32 \text{ m/s}^2$  usually detrain in the upper troposphere. Each of the four levels nearest the surface is therefore in principle able to generate deep and shallow outflow modes. A fraction  $f_{\text{deep}}$  of the parcel mass  $m_{p,i}$  defined earlier is assigned to the deep mode, while the remaining parcel mass is assigned to the shallow mode. The deep outflow fraction  $f_{\text{deep}}$  is specified to be an increasing function of  $R_{\text{mean}}$ , using the same formalism used to calculate the moist enthalpy spectrum width  $dk_m$ . The coefficients used in the expressions for  $f_{\text{deep}}$  are given in Table A1, and its dependence on  $R_{\text{mean}}$  is shown in Figure A1.

#### A4. Fractional Conversion of Excess Condensate to Precipitation

As updraft parcels rise in the atmosphere, they sometimes generate condensate (always assumed to be liquid) in excess of a prescribed maximum  $r_{l,\text{max}}$ . This maximum is specified as a function of temperature, and for all updraft parcel temperatures warmer than 245 K is equal to 1.5 g/kg. At colder temperatures, it increases to 4 g/kg. Some fraction  $f_{\text{precip}}$  of the updraft condensate in excess of  $r_{l,\text{max}}$  is converted to precipitation. The remainder is assumed to detrain into the background atmosphere (except when the background atmosphere at that particular height is saturated, in which case  $f_{\text{precip}} = 1$ ). The efficiency  $f_{\text{precip}}$  with which updraft condensate is converted to precipitation increases with rain rate. We again use the same sigmoidal formalism for  $f_{\text{precip}}$  as used for  $dk_m$ , with the coefficients listed in Table A1.

#### Acknowledgments

This research was supported by a Discovery Grant from the Natural Sciences and Engineering Research Council of Canada (NSERC). The CERES data were obtained from the NASA Langley Research Center Atmospheric Science Data Center.

#### References

- Ahijevych, D. A., C. A. Davis, R. E. Carbone, and J. D. Tuttle (2004), Initiation of precipitation episodes relative to elevated terrain, *J. Atmos. Sci.*, *61*, 2763–2769.
- Bacmeister, J. T., M. F. Wehner, R. B. Neale, A. Gettelman, C. Hannay, P. H. Lauritzen, J. M. Caron, and J. E. Truesdale (2013), Exploratory high-resolution climate simulations using the Community Atmosphere Model (CAM), *J. Clim.*, doi:10.1175/JCLI-D-13-00387.1.
- Bechtold, P., E. Bazile, F. Guichard, P. Mascart, and E. Richard (2001), A mass-flux convection scheme for regional and global models, *Q. J. R. Meteorol. Soc.*, *127*, 869–886.
- Bechtold, P., J.-P. Chaboureaud, A. Beljaars, A. K. Betts, M. Kohler, M. Miller, and J.-L. Redelsperger (2004), The simulation of the diurnal cycle of convective precipitation over land in a global model, *Q. J. R. Meteorol. Soc.*, *130*, 3119–3137.
- Betts, A. K., and C. Jakob (2002), Study of diurnal cycle of convective precipitation over Amazonia using a single column model, *J. Geophys. Res.*, *107*(D23), 4732, doi:10.1029/2002JD002264.
- Chakraborty, A. (2010), The skill of ECMWF medium-range forecasts during the year of tropical convection 2008, *Mon. Weath. Rev.*, *138*, 3787–3805.
- Chao, W. C. (2013), Catastrophe-concept-based cumulus parameterization: Correction of systematic errors in the precipitation diurnal cycle over land in a GCM, *J. Atmos. Sci.*, *70*, 3599–3614.
- Clark, A. J., W. A. Gallus, and T.-C. Chen (2007), Comparison of the diurnal precipitation cycle in convection-resolving and non-convection-resolving mesoscale models, *Mon. Weath. Rev.*, *135*, 3456–3473.
- Cohen, J. C. P., A. F. S. M. Dias, and C. A. Nobre (1995), Environmental conditions associated with Amazonian squall lines: A case study, *Mon. Weath. Rev.*, *123*, 3163–3174.
- Dai, A. (2006), Precipitation characteristics in eighteen coupled climate models, *J. Clim.*, *19*, 4605–4630.
- Dai, A., and K. E. Trenberth (2004), The diurnal cycle and its depiction in the Community Climate System Model, *J. Clim.*, *17*, 930–951.
- Dai, A., F. Giorgio, and K. E. Trenberth (1999), Observed and model-simulated diurnal cycles of precipitation over the contiguous United States, *J. Geophys. Res.*, *104*(D6), 6377–6402.
- da Rocha, R. P., C. A. Morales, S. V. Cuadra, and T. Ambrizzi (2009), Precipitation diurnal cycle and summer climatology assessment over South America: An evaluation of Regional Climate Model version 3 simulations, *J. Geophys. Res.*, *114*, D10108, doi:10.1029/2008JD010212.
- de Arellano, J.-V., B. Gioli, F. Miglietta, H. J. J. Jonker, H. K. Baltink, R. W. A. Hutjes, and A. A. M. Holtslag (2004), Entrainment process of carbon dioxide in the atmospheric boundary layer, *J. Geophys. Res.*, *109*, D18110, doi:10.1029/2004JD004725.

- Folkens, I. (2009), A one-dimensional cloud model with trimodal convective outflow, *J. Clim.*, *22*, 6437–6455.
- Garreaud, R. D., and J. M. Wallace (1997), The diurnal march of convective cloudiness over the Americas, *Mon. Weath. Rev.*, *125*, 3157–3171.
- Gent, P. R., et al. (2011), The Community Climate System Model version 4, *J. Clim.*, *24*, 4973–4991.
- Grell, G. (1993), Prognostic evaluation of assumptions used by cumulus parameterizations, *Mon. Weath. Rev.*, *121*, 764–787.
- Guichard, F., et al. (2004), Modelling the diurnal cycle of deep precipitating convection over land with cloud-resolving models and single-column models, *Q. J. R. Meteorol. Soc.*, *130*, 3139–3172.
- Hack, J. J. (1994), Parameterization of moist convection in the National Center for Atmospheric Research Community Climate Model (CCM2), *J. Geophys. Res.*, *99*, 5551–5568.
- Jakob, C., and A. P. Siebesma (2003), A new subcloud model for mass-flux convection schemes: Influence on triggering, updraught properties and model climate, *Mon. Weath. Rev.*, *131*, 2765–2778.
- Kay, J. E., et al. (2012), Exposing global cloud biases in the Community Atmosphere Model (CAM) using satellite observations and their corresponding instrument simulators, *J. Clim.*, *25*, 5190–5207.
- Khairoutdinov, M., and D. Randall (2006), High-resolution simulation of shallow-to-deep convection transition over land, *J. Atmos. Sci.*, *63*, 3421–3436.
- Kidd, C., E. Dawkins, and G. Huffman (2013), Comparison of precipitation derived from the ECMWF operational forecast model and satellite precipitation datasets, *J. Hydrometeorol.*, *14*, 1463–1482.
- Kim, J.-E., and M. J. Alexander (2013), Tropical precipitation variability and convectively coupled equatorial waves on submonthly time scales in reanalyses and TRMM, *J. Clim.*, *26*, 3013–3030.
- Kim, K.-M., W. K. M. Lau, Y. C. Sud, and G. K. Walker (2010), Influence of aerosol-radiative forcings on the diurnal and seasonal cycles of rainfall over West Africa and eastern Atlantic Ocean using GCM simulations, *Clim. Dyn.*, *35*, 115–126, doi:10.1007/s00382-010-0750-1.
- Kley, D., J. M. Russell III, and C. Phillips (2000), SPARC assessment of upper tropospheric and stratospheric water vapour, *WMO Tech. Doc.*, *1043*, SPARC Tech. Rep. 2, WCRP, 113.
- Kousky, V. E. (1980), Diurnal rainfall variation in northeast Brazil, *Mon. Weath. Rev.*, *108*, 488–498.
- Leary, C. A., and R. Houze (1979), Melting and evaporation of hyrometeors in precipitation from the anvil clouds of deep tropical convection, *J. Atmos. Sci.*, *36*, 669–679.
- Lee, M.-I., et al. (2007), Sensitivity to horizontal resolution in the AGCM simulations of warm season diurnal cycle of precipitation over the United States and Northern Mexico, *J. Clim.*, *20*, 1862–1881.
- Lee, M.-I., S. D. Schubert, M. J. Suarez, J.-K. E. Schemm, H.-L. Pan, J. Han, and S.-H. Yoo (2008), Role of convection triggers in the simulation of the diurnal cycle of precipitation over the United States Great Plains in a general circulation model, *J. Geophys. Res.*, *113*, D02111, doi:10.1029/2007JD008984.
- Liang, X.-Z., L. Li, A. Dai, and K. E. Kunkel (2004), Regional climate model simulation of summer precipitation diurnal cycle over the United States, *Geophys. Res. Lett.*, *31*, L24208, doi:10.1029/2004GL021054.
- Liu, Z., D. Ostrenga, W. Teng, and S. Kempler (2012), Tropical Rainfall Measuring Mission (TRMM) precipitation data and services for research and applications, *B. Am. Met. Soc.*, *93*, 1317–1325.
- Mapes, B. E., and R. B. Neale (2011), Parameterizing convective organization to escape the entrainment dilemma, *J. Adv. Model. Earth Syst.*, *3*, M06004, doi:10.1029/2011MS000042.
- May, P. T., C. N. Long, and A. Protat (2012), The diurnal cycle of the boundary layer, convection, clouds, and surface radiation in a coastal monsoon environment (Darwin, Australia), *J. Clim.*, *25*, 5309–5326.
- Mitovski, T., and I. Folkens (2013), Anomaly patterns about strong convective events in the tropics and mid-latitudes: Observations from radiosondes and surface weather stations, *J. Geophys. Res. Atmos.*, *118*, doi:10.1002/2013JD020447.
- Neale, R. B., J. Richter, S. Park, and P. H. Lauritzen (2013), The mean climate of the Community Atmosphere Model (CAM4) in forced SST and fully coupled experiments, *J. Clim.*, *26*, 5150–5168.
- Nesbitt, S. W., and E. Zipser (2003), The diurnal cycle of rainfall and convective intensity according to three years of TRMM measurements, *J. Clim.*, *16*, 1456–1475.
- Ploshay, J. J., and N. C. Lau (2010), Tropical rainfall and circulation during boreal summer with a high-resolution GCM, *Mon. Wea. Rev.*, *138*, 3434–3453.
- Rio, C., F. Hourdin, J.-Y. Grandpeix, and J.-P. Lafore (2009), Shifting the diurnal cycle of parameterized deep convection over land, *Geophys. Res. Lett.*, *36*, L07809, doi:10.1029/2008GL036779.
- Salio, P., M. Nicolini, and E. J. Zipser (2007), Mesoscale convective systems over southeastern South American low-level jet, *Mon. Weath. Rev.*, *135*, 1290–1309.
- Sato, T., H. Miura, M. Satoh, Y. N. Takayabu, and Y. Q. Wang (2009), Diurnal cycle of precipitation in the tropics simulated in a global cloud-resolving model, *J. Clim.*, *22*, 4809–4826.
- Soden, B. J. (2000), The diurnal cycle of convection, clouds, and water vapor in the tropical upper troposphere, *Geophys. Res. Lett.*, *27*, 2173–2176, doi:10.1029/2000GL011436.
- Stratton, R. A., and A. J. Stirling (2012), Improving the diurnal cycle of convection in GCMs, *Q. J. R. Meteorol. Soc.*, *138*, 1121–1134.
- Taylor, K. E. (2001), Summarizing multiple aspects of model performance in a single diagram, *J. Geophys. Res.*, *106*, 7183–7192, doi:10.1029/2000JD900719.
- Taylor, P. C. (2012), Tropical outgoing longwave radiation and longwave cloud forcing diurnal cycles from CERES, *J. Atmos. Sci.*, *69*, 3652–3669.
- Tompkins, A. M. (2001a), Organization of tropical convection in low vertical wind shears: The role of water vapor, *J. Atmos. Sci.*, *58*, 529–545.
- Tompkins, A. M. (2001b), Organization of tropical convection in low vertical wind shears: The role of cold pools, *J. Atmos. Sci.*, *58*, 1650–1672.
- Tulich, S. N., and G. N. Kiladis (2012), Squall lines and convectively coupled gravity waves in the tropics: Why do most cloud systems propagate westward?, *J. Atmos. Sci.*, *69*, 2995–3012.
- Velasco, I., and J. M. Fritsch (1987), Mesoscale convective complexes in the Americas, *J. Geophys. Res.*, *92*, 9591–9613, doi:10.1029/JD092iD08p09591.
- Wielicki, B. A., B. R. Barkstrom, E. F. Harrison, R. B. Lee III, G. L. Smith, and J. E. Cooper (1996), Clouds and the Earth's Radiant Energy System (CERES): An Earth observing system experiment, *Bull. Amer. Meteor. Soc.*, *77*, 853–868.
- Xie, S., M. Zhang, J. S. Boyle, R. T. Cederwall, G. L. Potter, and W. Lin (2004), Impact of a revised convective triggering mechanism on community atmosphere model, version 2, simulations: Results from short-range weather forecasts, *J. Geophys. Res.*, *109*, D14102, doi:10.1029/2004JD004692.

- Yamada, T. J., M. Lee, M. Kanamitsu, and H. Kanamaru (2012), Diurnal characteristics of rainfall over the contiguous United States and Northern Mexico in the dynamically downscaled reanalysis dataset (US10), *J. Hydrometeorol.*, *13*, 1142–1148.
- Yang, G.-Y., and J. Slingo (2001), The diurnal cycle in the tropics, *Mon. Weath. Rev.*, *129*, 784–801.
- Yuan, W., R. Yu, M. Zhang, W. Lin, J. Li, and Y. Fu (2013), Diurnal cycle of summer precipitation over subtropical East Asia in CAM5, *J. Clim.*, *26*, 3159–3172.
- Zhang, G. J. (2003), Roles of tropospheric and boundary layer forcing in the diurnal cycle of convection in the U.S. Southern Great Plains, *Geophys. Res. Lett.*, *30*(24), 2281, doi:10.1029/2003GL018554.
- Zhang, G. J., and N. A. McFarlane (1995), Sensitivity of climate simulations to the parameterization of cumulus convection in the Canadian Climate Centre general circulation model, *Atmos.-Ocean*, *33*, 407–446.
- Zhang, Y., and S. A. Klein (2010), Mechanisms affecting the transition from shallow to deep convection over land: Inferences from observations of the diurnal cycle collected at the ARM Southern Great Plains site, *J. Atmos. Sci.*, *67*, 2943–2959.